ELSEVIER

Coordination Chemistry Reviews
171 (1998) 439–459

COORDINATION CHEMISTRY REVIEWS

Metal-to-ligand charge-transfer photochemistry: quantum chemistry and dynamics of the systems $RM(CO)_3(DAB)$ (M = Mn; R = H, methyl, ethyl; M = Re, R = H, DAB = 1,4-diaza-1,3-butadiene)

D. Guillaumont [a,*], K. Finger [b], M. R. Hachey [c], C. Daniel [a]

[a] *Laboratoire de Chimie Quantique, UPR 139 du CNRS, Université Louis Pasteur, 4 Rue Blaise Pascal 67000 Strasbourg, France*
[b] *Institut für Physikalische und Theoretische Chemie, Freie Universität, 14195 Berlin, Germany*
[c] *University of Fredericton, Fredericton, N.B., Canada*

Received 7 July 1997; received in revised form 14 August 1997; accepted 19 November 1997

Contents

* Corresponding author.

PII S0010-8545(98)00024-1

Abstract

The photodissociation dynamics of the model system $HMn(CO)_3$(α-diimine), representative of a class of transition metal complexes characterized by low-lying metal-to-ligand charge-transfer excited states, is reported for the following elementary processes: (i) absorption from the singlet electronic ground state to the low-lying singlet excited states; (ii) dissociation on nine kinetically coupled potentials corresponding to the low-lying singlet excited states and to the upper triplet dissociative state; (iii) photodissociation under visible irradiation; (iv) photodissociation under UV irradiation. By extension of the strategy applied with success to small di- and tri-atomic molecules to multidimensional transition metal complexes, the dynamics are simulated using a time-dependent wave packet propagation technique on ab initio CASSCF/CCI potentials calculated along the Mn–H elongation for the singlet/triplet excited states. The nature of the photoactive excited states is determined without ambiguity, as well as the time scales and some important features of the absorption spectrum (either in the UV region or in the visible region). On the basis of this one-dimensional complete study and on the calculation of the lowest excited states in $RM(CO)_3$(DAB) (M = Mn and R = methyl, ethyl; M = Re, R = H) a tentative rationalization of the photochemical and photophysical properties of this class of molecules is proposed. © 1998 Elsevier Science S.A.

Keywords: MLCT Photochemistry; Quantum Chemistry; Excited state dynamics

1. Introduction

According to a number of experiments, the family of α-diimine mono- and di-nuclear transition metal carbonyls show a dual deactivation process: they either (i) photodissociate, leading to highly reactive intermediates, or (ii) manifest the photophysics (including spectroscopy) of metal-to-ligand charge-transfer (MLCT) complexes [1–6]. These two distinct behaviors may be used to promote selective applications like catalytic activity or energy/electron transfers. Quite recently, spectroscopy, photophysics and photochemistry of a series of $M(L)(CO)_3$(α-diimine) complexes (M = Mn, Re), in which L represents a metal fragment or alkyl groups bound to the metal by a high-lying σ orbital, have been studied in detail [7–9]. From these experimental studies, it was concluded that the absorption spectra result mainly from the $d_\pi(M) \rightarrow \pi^*$(α-diimine) (MLCT) transitions, and that emission and homolysis reactions take place from a close low-lying $\sigma(M–L) \rightarrow \pi^*$(α-diimine) (^{3}LLCT) excited state.

In classical experiments, with long and monochromatic laser pulses, the UV–visible spectra obtained are usually broad, featureless and without detailed assignments. More sophisticated fast time-resolved infrared (TRIR) spectroscopy has been developed to follow the behavior of short lifetime intermediates [10]. However, according to recent pico-/femto-second experiments on $[CpFe(CO)_2]_2$ [11–15] there is considerable difficulty in distinguishing the early stage of the photodissociation (in the femtosecond time scale) from the vibrational relaxation effects.

The exploration of the potential energy surfaces (PESs) associated with the excited states contributing to the absorption/emission spectra and/or participating in the

photodissociation process, by means of the time-dependent theory, offers promise in helping to understand and analyze the sequence of events between the initial excitation and the formation of the primary products.

In recent simulations, we extended the model proposed by Imre and coworkers [16–20] for competitive bond breaking from simple linear triatomic ABC systems

$$AB+C\leftarrow[ABC]^*\rightarrow A+BC \quad (1)$$

to large transition metal complexes. The photochemistry of organometallics is governed by intramolecular vibrational energy redistribution (IVR), intersystem crossing (ISC), internal conversion (IC), direct dissociation (DD) on repulsive PESs in the femtosecond time scale or indirect dissociation (ID). This complex network of elementary processes has been considered under the time-dependent approach for a series of model systems, each representative of a class of molecules [21–26]. The aim of this contribution is to report recent advances, based on quantum chemical calculations coupled with simulation of the photodissociation dynamics, in the field of MLCT transition metal compounds. We have shown, in a preliminary theoretical study of the photodissociation dynamics of $HMn(CO)_3(DAB)$, that the key to the understanding of the photochemical behavior of the title complexes is the relative position of the ^{3}LLCT ($\sigma_{M-R}\rightarrow\pi^*_{dab}$) state (responsible for the M–R bond homolysis) with respect to the lowest ^{3}MLCT states corresponding to $d\pi\rightarrow\pi^*_{dab}$ excitations [27–30]. This work reports a complete one-dimensional simulation of the photodissociation dynamics along the Mn–H bond elongation. It was performed on the low-lying non-adiabatically coupled singlet potentials (^{1}LLCT and ^{1}MLCT) which are also coupled with low-lying triplet potentials (^{3}LLCT and ^{3}MLCT) through spin–orbit coupling. In order to rationalize the photochemical/photophysical behavior of this class of molecules, state correlation diagrams connecting the low-lying singlet and triplet excited states of $RMn(CO)_3(DAB)$ (R = H, methyl, ethyl) to the corresponding states of Mn–R bond homolysis primary products $R+Mn(CO)_3(DAB)$ are compared for the different fragments R. An analysis of spectroscopic properties of this class of compounds is based on the state correlation diagrams and on the whole dynamics simulation of the model system $HMn(CO)_3(DAB)$. A preliminary investigation of the influence of the metal center is undertaken through the calculation of the low-lying triplet and singlet excited states of $HRe(CO)_3(DAB)$.

2. Model and techniques

2.1. Model systems

The choice of the model systems has been motivated by experiments of the Amsterdam group [1–9] and by our own preliminary studies based on the analysis of the triplet potential energy curves calculated for the breaking of the metal–hydrogen bond and the departure of a carbonyl ligand in the model system $HMn(CO)_3(DAB)$ [27–30].

The photodissociation dynamics have been simulated for the following primary reaction:

$$HMn(CO)_3(DAB) \xrightarrow{h\nu} H + Mn(CO)_3(DAB) \quad (2)$$

The calculations have been performed under C_s symmetry constraint for the $^1A'$ electronic ground state corresponding to the $(\sigma)^2(3dx^2-y^2)^2(3d_{yz})^2(3d_{xz})^2$ electronic configuration and for the low-lying $^{1,3}A'$ excited states corresponding to $(\sigma)^2(3d_{x^2-y^2})^2(3d_{yz})^2(3d_{xz})^1(\pi^*_{dab})^1$, $(\sigma)^2(3d_{x^2-y^2})^1(3d_{yz})^2(3d_{xz})^2(\pi^*_{dab})^1$ and $(\sigma)^1(3d_{x^2-y^2})^2(3d_{yz})^2(3d_{xz})^2(\pi^*_{dab})^1$ electronic configurations. The equilibrium conformations are depicted in Fig. 1.

Idealized geometries have been deduced from the ground state structures of $MnCl(CO)_3(DAB)$ [31] and of $HMn(CO)_5$ [32]. The geometrical parameters details are given elsewhere [33]. Geometrical relaxation effects in the lowest ^{3}MLCT state and in the ^{3}LLCT state have been studied through gradient-CASSCF optimizations for the hydride complex at the equilibrium (in the Franck–Condon region) and in the asymptotic region of the Mn–H bond homolysis. The main structural deformations consist of an elongation of the Mn–CO_{ax} bond in the lowest a^3A' ($3d_{xz} \rightarrow \pi^*_{dab}$) excited state (1.918 Å in the ground state vs. 2.235 Å in the excited state) and in an elongation of the Mn–H bond in the d^3A' ($\sigma_{M-R} \rightarrow \pi^*_{dab}$) excited state (1.625 Å in the ground state vs. 1.946 Å in the excited state). The main angular deformations are less than 10° and other interatomic distances change very little [34,35]. Since we are interested by fast events (vertical transitions in the Franck–Condon domain, direct dissociations occurring in the femtosecond time

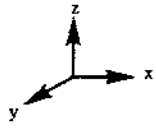

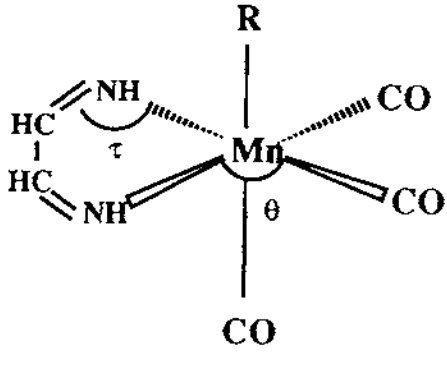

Fig. 1. Idealized geometry of $RMn(CO)_3(DAB)$ (R = H, Me, Et).

scale and ISCs occurring in the picosecond time scale) a systematic geometry optimization of the excited states has not been performed. In any cases, the geometrical deformations on going from the equilibrium to the dissociated fragments $H+Mn(CO)_3(DAB)$ are not sufficiently significant to justify costly gradient calculations at a correlated level. Clearly, investigation of other photophysical properties connected to excited states with long lifetimes (emission spectra) would need to take relaxation effects into account, particularly in the low-lying triplet excited states.

2.2. Excited states calculations

CASSCF [36] calculations, averaged over the low-lying states of a given symmetry and spin, were performed in order to generate a set of molecular orbitals used in a subsequent multireference CI [37]. Our interest centered mostly on the lowest excited states corresponding to $d\rightarrow d$, $d\rightarrow\pi^*_{dab}$ and $\sigma\rightarrow\pi^*_{dab}$ excitations. Eight electrons were correlated (the 3d electrons and the two electrons involved in the M–R bond) in either ten (R = H, methyl) or nine (R = ethyl) orbitals corresponding to the 3d and 4d orbitals which correlate them, the σ_{M-R} and σ^*_{M-R} orbitals (σ_{M-R} and σ^*_{M-R} orbitals respectively denote the molecular orbitals that are bonding and antibonding with respect to the M–R bond) and the lowest π^*_{dab} orbital localized on the DAB group. For each electronic state a monoreference CCI calculation was followed by a multireference calculation, including all configurations with a coefficient larger than 0.08 in the monoreference CI. Single and double excitations to all virtual orbitals, except the counterparts of the carbonyls and diimine 1s and the metal 1s, 2s and 2p orbitals, are included. The basis sets used are detailed elsewhere [33]. All electron calculations have been performed for the manganese complexes, whereas relativistic effective core potentials [38,39] (in the small core approximation) have been used for the rhenium complex.

2.3. State correlation diagrams

A step forward in understanding the mechanism of photochemical reactions of organometallics was the use of state correlation diagrams [40–42]. State correlation diagrams are rather crude approximations to the PESs that connect the reactants to the primary photochemical products. In this approach, one needs to identify first the ground state and low-lying excited states of the reactants and of the primary products. This can be done by either a qualitative energy level scheme or ab initio calculations. State correlation diagrams for $RMn(CO)_3(DAB)$ (R = H, methyl, ethyl) and its primary products $R+Mn(CO)_3(DAB)$ have been built on the basis of spin and symmetry conservation rules [43]. The relative CASSCF/CCI energies of the different molecules in the ground state and in the low-lying singlet and triplet states were used.

2.4. PESs

In its elementary form the photochemical behavior of the molecule under investigation can be modeled as a pseudotriatomic system with two collinear dissociative

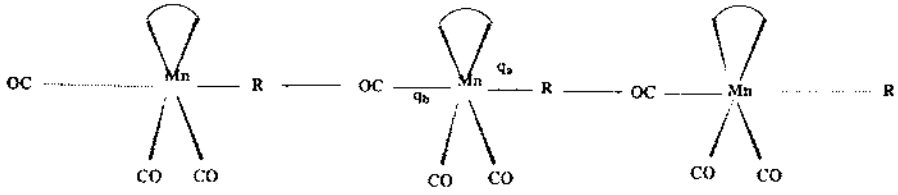

Scheme 1.

bonds, q_a=[Mn–H] and q_b=[Mn–CO_{ax}]. In the present work, however, only the simulation along the q_a bond will be reported. A two-dimensional simulation is reported elsewhere [44]. All other spectator modes are decoupled in this zero-order approximation. This mode decoupling should be reasonable, at least for ultrafast time scales (in the order of 100 fs) when initial energy remains stored in the dissociative bond(s). The photodissociation of $HMn(CO)_3$(α-diimine) (Eq. (2)) has been studied under C_s symmetry constraint (Scheme 1).

The potentials for the electronic ground states and the lowest excited states of $HMn(CO)_3$(DAB) molecules are modeled by fitting analytical functions to CASSCF/CCI ab initio points, with additional smoothing to avoid any obvious artefacts, such as shallow minima in the asymptotic domain. Details of the ab initio calculations (basis sets, size of the CI, CASSCF reference wavefunctions) are detailed elsewhere [44]. The choice of the electronic states selected for simulating the dynamics is governed by the oscillator strengths associated to the low-lying singlet states. The first step of the simulation is the construction of the theoretical absorption spectrum. For this, one needs the potentials corresponding to the electronic ground state and to the lowest spin (singlet) and symmetry-allowed transitions. Photodissociation dynamics investigation is based on potentials corresponding to bound and dissociative electronic states either coupled non-adiabatically (singlets) or coupled by spin–orbit interaction (singlets–triplets).

2.5. *Photodissociation dynamics*

The photoabsorption and the subsequent bond breaking described in the reaction given in Eq. (2) are simulated by propagation of selected wavepackets $\Psi_e(q_a, t)$ on the potentials corresponding to the e excited states. The time evolution of the wavepackets is obtained by solving the time-dependent Schrödinger equation:

$$i\hbar \frac{\partial}{\partial t} \Psi_e(q_a, t) = [T_{nu} + V_e]\Psi_e(q_a, t) \tag{3}$$

with the initial conditions

$$\Psi_e(q_a, t=0) = \mu_e \Phi_{gs,0}(q_a) \tag{4}$$

where μ_e is the electronic transition moment between the ground state (gs) and the excited state e. $\Phi_{gs,0}(q_a)$ represents the one-dimensional vibrational ground wavefunc-

tion of the electronic ground state evaluated through the Fourier grid Hamiltonian method [45,46]. The solution of the time-dependent Schrödinger equation (Eq. (3)) is obtained by the second-order-differential propagation scheme with $\Delta t = 7.0 \times 10^{-3}$ fs [47].

The absorption spectrum σ_{tot} is obtained by the Fourier transform of the total autocorrelation function $S_{tot}(t)$ summed over the individual autocorrelation functions corresponding to each excited state e

$$\sigma_{tot}(\omega) \propto \omega \int_{-\infty}^{+\infty} dt\, e^{i(E_i+\omega)t} S_{tot}(t) \tag{5}$$

where

$$S_{tot}(t) = \sum_{e} \langle \Psi_e(0) | \Psi_e(t) \rangle \tag{6}$$

and E_i represents the energy of the initial wave packet on the electronic state e.

The kinetic part of the Hamiltonian of the system, expressed in bond coordinates, is given by

$$T_{nu} = -\frac{\hbar^2}{2\mu_a} \frac{\partial^2}{\partial q_a^2} \tag{7}$$

where μ_a is the reduced mass corresponding to the bond q_a. The propagations are based on representations of $\Psi_e(q_a, t)$ on one-dimensional grids corresponding to the reaction coordinate with the following parameters: $q_{a_i} = q_{a_0} + (i-1)\Delta q_a$, $q_{a_0} = 1.0$ a.u., $\Delta q_a = 0.1$ a.u. with $1 \leqslant i \leqslant 512$.

When the spin–orbit interaction between two electronic states k and k', defined by the spin–orbit coupling diabatic matrix element

$$V^d_{kk'} = \langle \Xi^{el}_k | \hat{H}_{so} | \Xi^{el}_{k'} \rangle \tag{8}$$

is included for the description of singlet to triplet radiationless transitions, the time evolution of the wavepackets $\Psi_k(q_a, t)$ in the diabatic representation is evaluated by solving a set of coupled time-dependent Schrödinger equations [23,24]

$$i\hbar \frac{\partial \Psi_k}{\partial t}(q_a, t) = H_k \Psi_k(q_a, t) + \sum_{k \neq k'} V^d_{kk'} \Psi_{k'} \tag{9}$$

with specific initial conditions and a constant value for the spin–orbit coupling potential calculated, using the effective one-electron operator, on the basis of a restricted full CI scheme as described in detail in Ref. [48].

When several potentials are coupled non-adiabatically (symmetry-avoided crossings), the time evolution of the wave packet $\Psi_k(q_a, t)$ in the diabatic representation is obtained by solving the set of coupled time-dependent Schrödinger equations (Eq. (9)), where $V^d_{kk'}$ are the diabatic potential couplings obtained by a unitary transformation which shifts the kinetic couplings of the adiabatic representation into the potential matrix [29]. The kinetic couplings are expected to be sharply

peaked around the avoided crossings regions and are approximated by asymmetric Lorentzians.

2.6. Properties

Several techniques are used to analyze the resulting wavepackets and to derive various properties useful for comparisons with experimental data and predictions for future sophisticated experiments. Namely, it is possible to calculate: movies of the densities, branching ratio for two competing product channels on a given electronic state, autocorrelation functions, emission/absorbtion spectra. Descriptions of the techniques used to calculate these properties are given elsewhere [21–26].

3. Results and discussion

3.1. Excited states

3.1.1. Excited states of $RMn(CO)_3(DAB)$ (R = H, methyl, ethyl)

The calculated vertical excitation energies of the lowest $^{1,3}A'$ states of $RMn(CO)_3(DAB)$ (R = H, methyl, ethyl) are reported in Table 1.

The lowest singlet excited states correspond to one-electron excitations, either from the metal-centered 3d orbitals or from the metal–radical σ_{Mn-R} bonding orbital to the low-lying vacant π^*_{dab} orbital of the diimine group. The first three singlet excited states range between 21 060 and 37 950 cm^{-1} (R = H), 20 430 and 28 200 cm^{-1} (R = methyl) and 15 850 and 26 240 cm^{-1} (R = ethyl). The corresponding triplet excited states range between 15 090 and 34 390 cm^{-1} (R = H), 12 730 and 22 900 cm^{-1} (R = methyl) and 11 080 and 16 200 cm^{-1} (R = ethyl). The principal trend on going from the hydride, to the methyl, and the substituted ethyl complexes is a lowering of the excited states energies. This general trend is more pronounced on going from the hydride to the methyl than from the methyl to the ethyl complex. This is mainly attributed to a stabilization of the vacant π^*_{dab} orbital and, consequently, to the weakening of the Mn–R bond resulting from the replacement of hydrogen by a methyl or an ethyl radical. The weakening of the Mn–R bond with respect to the ligand R is further illustrated by an even more pronounced lowering of the ^{1}LLCT states $\sigma_{Mn-R} \rightarrow \pi^*_{dab}$ with respect to the MLCT states to $d \rightarrow \pi^*_{dab}$. The second significant difference between the hydride complex and the methyl- or ethyl-substituted molecules is a strong mixing between the low-lying ^{3}MLCT ($3d_{xz} \rightarrow \pi^*_{dab}$) and the ^{3}LLCT ($\sigma_{Mn-R} \rightarrow \pi^*_{dab}$) states and between the two lowest ^{1}MLCT ($3d_{xz} \rightarrow \pi^*_{dab}$) and ^{1}MLCT ($3d_{x^2-y^2} \rightarrow \pi^*_{dab}$) states. The different behaviors exhibited by the singlet and triplet sets may be explained by the strong interaction between the electronic ground state and the ^{1}LLCT state in the three molecules. Since closed shell configurations cannot give rise to triplet multiplicity, the ground state cannot interact with the triplet states directly. The interaction of the singlet ground state with the ^{1}LLCT appears to inhibit mixing between ^{1}LLCT and ^{1}MLCT, in contrast to the mixing behavior in their triplet counterparts. The

Table 1
Calculated CASSCF/CCI vertical excitation energies (cm^{-1}) to the lowest $^{1,3}A'$ excited states of $RMn(CO)_3(DAB)$ (R = H, methyl, ethyl)

	One-electron excitation in the principal configurations	R = H	One-electron excitation in the principal configurations	R = methyl	One-electron excitation in the principal configurations	R = ethyl
$a^1A' \rightarrow a^3A'$	^{3}MLCT $3d_{xz} \rightarrow \pi^*_{dab}$ (0.90)	15 090	^{3}(MLCT/LLCT) $3d_{xz} \rightarrow \pi^*_{dab}$ (0.63) $\sigma_{Mn\ R} \rightarrow \pi^*_{dab}$ (0.65)	12 730	^{3}(LLCT/MLCT) $\sigma_{Mn-R} \rightarrow \pi^*_{dab}$ (0.66) $3d_{xz} \rightarrow \pi^*_{dab}$ (0.61)	11 080
$a^1A' \rightarrow b^3A'$	^{3}MLCT $3d_{x^2-y^2} \rightarrow \pi^*_{dab}$ (0.88)	19 200	^{3}MLCT $3d_{x^2-y^2} \rightarrow \pi^*_{dab}$ (0.90)	16 820	^{3}(MLCT/LLCT) $3d_{x^2-y^2} \rightarrow \pi^*_{dab}$ (0.69) $\sigma_{Mn-R} \rightarrow \pi^*_{dab}$ (0.58)	12 280
$a^1A' \rightarrow b^1A'$	^{1}MLCT $3d_{x^2-y^2} \rightarrow \pi^*_{dab}$ (0.90)	21 060 **f=0.03**	^{1}MLCT $3d_{xz} \rightarrow \pi^*_{dab}$ (0.68) $3d_{x^2-y^2} \rightarrow \pi^*_{dab}$ (0.59)	20 430	^{1}MLCT $3d_{xz} \rightarrow \pi^*_{dab}$ (0.63) $3d_{x^2-y^2} \rightarrow \pi^*_{dab}$ (0.61)	15 580
$a^1A' \rightarrow c^1A'$	^{1}MLCT $3d_{xz} \rightarrow \pi^*_{dab}$ (0.75)	26 000 **f=0.39**	^{1}MLCT $3d_{x^2-y^2} \rightarrow \pi^*_{dab}$ (-0.67) $3d_{xz} \rightarrow \pi^*_{dab}$ (0.50)	23 050	^{1}MLCT $3d_{x^2-y^2} \rightarrow \pi^*_{dab}$ (-0.64) $3d_{xz} \rightarrow \pi^*_{dab}$ (-0.53)	17 560
$a^1A' \rightarrow c^3A'$	^{3}LLCT $\sigma_{Mn\ R} \rightarrow \pi^*_{dab}$ (0.89)	34 390	^{3}(LLCT/MLCT) $\sigma_{Mn-R} \rightarrow \pi^*_{dab}$ (0.69) $3d_{xz} \rightarrow \pi^*_{dab}$ (-0.57)	22 900	^{3}MLCT $3d_{x^2-y^2} \rightarrow \pi^*_{dab}$ (0.89)	16 200
$a^1A' \rightarrow d^1A'$	^{1}LLCT $\sigma_{Mn\ R} \rightarrow \pi^*_{dab}$ (0.80) GS (0.20)	37 950 **f=0.11**	^{1}LLCT $\sigma_{Mn\ R} \rightarrow \pi^*_{dab}$ (0.81) GS (0.24)	28 200	^{1}LLCT $\sigma_{Mn\ R} \rightarrow \pi^*_{dab}$ (0.82) GS (0.38)	26 240

mixing between the ^{3}MLCT ($3d_{xz} \rightarrow \pi^*_{dab}$) and ^{3}LLCT ($\sigma_{Mn-R} \rightarrow \pi^*_{dab}$) states is illustrated by the hybridization of the $3d_{xz}$ and $3d_{z^2}$ orbitals which increases the overlap between the metal center and the sp orbital of the radical R (methyl or ethyl).

In the molecular series, the ordering and nature of the low-lying singlet states are similar and well defined: the two lowest excited states have an MLCT character, the highest state has a ^{1}LLCT character with a contribution from the ground state. Therefore, the shape of the absorption spectrum should not differ drastically with the R ligands substitutions. Indeed, this is supported by experimental data for this family of molecules [1–9]. These experiments report an intense band in the visible corresponding to the absorption from the electronic ground state to one of the low-lying quasi-bound ^{1}MLCT states, and a weak shoulder in the UV region corresponding to the population of the weakly bound ^{1}LLCT state. According to the oscillator strengths calculated for the hydride (Table 1), the first intense band should correspond to a ^{1}MLCT state described mainly by the $3d_{xz} \rightarrow \pi^*_{dab}$ excitation. For the methyl complex, this state is calculated at 20 430 cm^{-1}, in excellent agreement with the experimental maximum around 500 nm which is observed for a number of α-diimine complexes.

Even if the spin-allowed absorption spectroscopy is not drastically affected by changing the nature of the radical substituents, other properties—particularly the photochemistry—may be considerably modified on going from the hydride, to the methyl and to the ethyl complex. A comparison of the composition of the low-lying triplet states in the R series ligands indicates a large change of character from the hydride to the methyl and to the ethyl radical. In the hydride, the two lowest ^{3}MLCT are nearly pure and well separated from the dissociative ^{3}LLCT state. In contrast, the methyl and ethyl compounds show a mixed character. This mixed ^{3}(LLCT/MLCT) nature for two of the three low-lying triplets may greatly influence the photochemical behavior. Moreover, the energy domain covered by the set of the three low-lying triplet excited states is considerably reduced on going from the hydride (19 300 cm^{-1}) to the methyl (10 200 cm^{-1}) and to the ethyl (5100 cm^{-1}) complex. This increase in the density of states may have a large influence on the early stage of the Mn–R bond homolysis for which energy barriers have been found for $HMn(CO)_3(DAB)$ [27,28].

3.1.2. Excited states of $HRe(CO)_3(DAB)$

The CASSCF/MRCI excitation energies to the lowest ^{1,3}A′ states of $HRe(CO)_3(DAB)$ are reported in Table 2. These results show two interesting features: (i) a lowering of the excitation energies on going from the manganese to the rhenium compound; (ii) a strong mixing between the so-called ^{1,3}MLCT ($5d_{xz} \rightarrow \pi^*_{dab}$) and ^{1,3}LLCT ($\sigma_{Re\ H} \rightarrow \pi^*_{dab}$) excited states. The lowering of the excited states is a direct consequence of the relativistic destabilization of the d shells, and of the stabilizing interaction between the vacant π^*_{dab} orbital and the $6p_z$ of the rhenium atom. The lowest singlet state is calculated at 15 250 cm^{-1} and corresponds to the nearly pure $5d_{x^2-y^2} \rightarrow \pi^*_{dab}$ excitation. The next singlet state matches well with an intense absorption band at around 20 000 cm^{-1} in the visible energy domain for this class of rhenium complexes. The mixed ^{1}(MLCT/LLCT) character of this

Table 2
Calculated CASSCF/CCI excitation energies (cm^{-1}) to the lowest $^{1,3}A'$ excited states of $HRe(CO)_3(DAB)$

Transition	One-electron excitation in the principal configurations	
$a^1A' \rightarrow a^3A'$	$5d_{xz} + \sigma_{Re\text{-}H} \rightarrow \pi^*_{dab}$ (0.71)	12 600
	$\sigma_{Re\ H} - 5d_{xz} \rightarrow \pi^*_{dab}$ (0.64)	
$a^1A' \rightarrow b^3A'$	$5d_{x^2-y^2} \rightarrow \pi^*_{dab}$ (0.90)	13 710
$a^1A' \rightarrow b^1A'$	$5d_{x^2-y^2} \rightarrow \pi^*_{dab}$ (0.91)	15 250
		$f = 0.0003$
$a^1A' \rightarrow c^1A'$	$5d_{xz} + \sigma_{Re\ H} \rightarrow \pi^*_{dab}$ (0.68)	21 721
	$\sigma_{Re\ H}$ $5d_{xz} \rightarrow \pi^*_{dab}$ (0.44)	$f = 0.32$
$a^1A' \rightarrow c^3A'$	$\sigma_{Re\ H} - 5d_{xz} \rightarrow \pi^*_{dab}$ (0.69)	27 650
	$5d_{xz} - \sigma_{Re\text{-}H} \rightarrow \pi^*_{dab}$ (0.59)	
$a^1A' \rightarrow d^1A'$	$\sigma_{Re\ H} - 5d_{xz} \rightarrow \pi^*_{dab}$ (0.64)	31 340
	$5d_{xz} + \sigma_{Re\text{-}H} \rightarrow \pi^*_{dab}$ (0.59)	$f = 0.12$

excited state could lead to a substantial distortions of the shape of the associated potential energy curves. This may explain some quite surprising photochemical behaviors of the rhenium complexes under irradiation in the visible. Indeed, according to recent experiments [49] a very efficient formation of radicals (supposing dissociative potentials) coupled with the detection of a long lifetime (250 ns) "$\sigma\pi^*$" excited state (characteristic of a bound state) has been observed. The highest calculated singlet excited state at 31 350 cm^{-1} shows a highly mixed LLCT/MLCT character.

According to the oscillator strengths reported in Table 2, the $a^1A' \rightarrow c^1A'$ transition should be the principal contributor to the intense visible absorption band characterizing this class of rhenium complexes [7–9]. The $a^1A' \rightarrow d^1A'$ transition should be responsible for a less intense band in the UV.

In contrast to its manganese homologue, the rhenium complex follows the same trends for the triplet states as for the singlet states. The lowest triplet excited state at 12 600 cm^{-1} is characterized by a strong MLCT/LLCT mixing. The next triplet state calculated at 13 710 cm^{-1} is nearly pure and corresponds to the $5d_{x^2-y^2} \rightarrow \pi^*_{dab}$ excitation. The highest calculated triplet state has an LLCT/MLCT character and lies at 27 650 cm^{-1}. The dominant MLCT character of the two a^3A' and b^3A' states (as in $RMn(CO)_3(DAB)$; R = H, methyl) should generate a situation resulting in avoided crossings with the "dissociative" c^3A' state, which has a large $\sigma_{Re\text{-}H} \rightarrow \pi^*_{dab}$ contribution. Investigations of state correlation diagrams and potential energy curves are necessary to corroborate this hypothesis. Further calculations are needed to estimate the spin–orbit splitting and the singlet–triplet interaction, which cannot be neglected in this heavy atom complex [48].[1]

[1]The spin–orbit interaction may account for a few thousand wavenumber units in the rhenium complex, according to the atomic splitting, to be compared with the largest value, of 107 cm^{-1} calculated between the a^3A' ($d_{xz} \rightarrow \pi^*_{dab}$) and d^1A' ($\sigma \rightarrow \pi^*_{dab}$) states of $HMn(CO)_3(DAB)$.

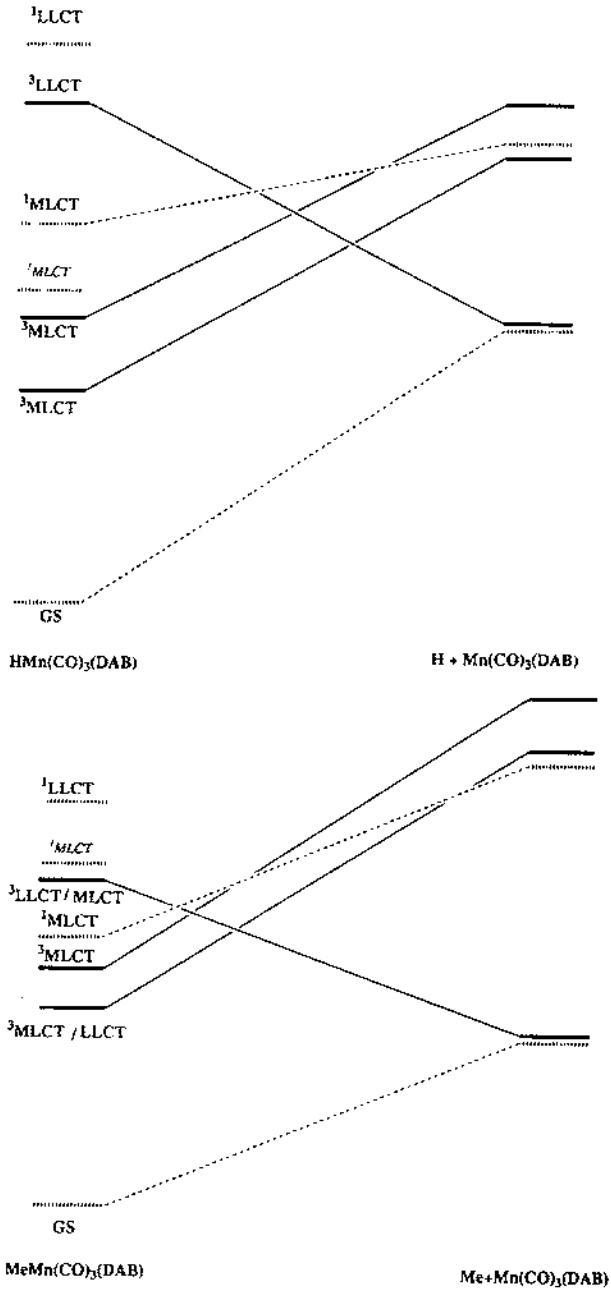

Fig. 2. State correlation diagrams based on CASSCF/CCI calculations connecting the electronic ground and lowest excited states of RMn(CO)$_3$(DAB) (a) R = H; (b) R = methyl; (c) R = ethyl (the same scales are used in the three diagrams).

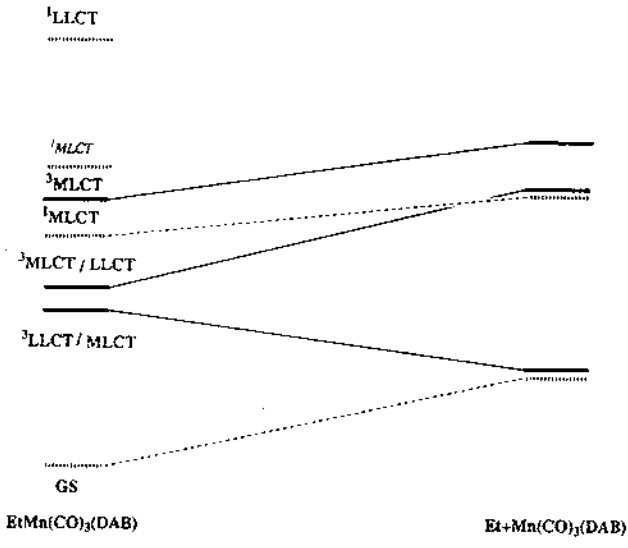

Fig. 2. (*continued*)

3.2. State correlation diagrams

The state correlation diagrams connecting the electronic ground state and the low-lying triplet excited states of $RMn(CO)_3(DAB)$ to the corresponding states of the primary products $R + Mn(CO)_3(DAB)$ are shown in Fig. 2(a) (R = H), Fig. 2(b) (R = methyl), Fig. 2(c) (R = ethyl). The same scale was used in the three figures.

The state correlation diagrams are based on the relative CASSCF/CCI energies of the electronic ground state and low-lying triplet states of $HMn(CO)_3(DAB)$. Fig. 2(a) shows an extreme situation where the ^{3}LLCT dissociative state is well separated from the low-lying quasi-bound pure ^{3}MLCT states. Consequently, the expected energy barriers generated by the avoided crossings along the Mn–H bond elongation [27–30] are too high to allow an efficient Mn–H homolysis under irradiation in the visible. Alternatives to Mn–H homolysis are the photodissociation of a carbonyl ligand, or emission to the electronic ground state from the low-lying, long lifetimes, triplet MLCT states. The ^{3}LLCT dissociative state stands in the upper part of the energy domain, well above the ^{1}MLCT (in bold letters in Fig. 2), which is accessible through allowed transitions from the electronic ground state (GS). An intermediate situation is depicted in Fig. 2(b), which shows the state correlation diagrams drawn for the methyl complex $MeMn(CO)_3(DAB)$. The shape of the associated potentials should be smoother and may allow the system to overcome the energy barriers generated by avoided crossings between the upper mixed ^{3}(LLCT/MLCT) state and the low-lying ^{3}MLCT and ^{3}(MLCT/LLCT) states. The homolysis of the Mn–R bond may appear as concurrent primary reactions to the carbonyl dissociation. The efficiency of both primary reactions will depend on factors like solvent effects or the nature of the diimine group, which have not been considered

in the present study. Finally, Fig. 2(c) shows the state correlation diagrams corresponding to the dissociation of the ethyl group in $EtMn(CO)_3(DAB)$. It indicates clearly that the ethyl dissociation reaction should be very efficient under irradiation in the visible. Indeed, the presence of the two mixed triplet states ^{3}(LLCT/MLCT) and ^{3}(MLCT/LLCT) in the lowest part of the energy domain prevent the occurrence of energy barriers generated by avoided crossings with the upper predominantly ^{3}MLCT state along this reaction coordinate. In addition, the relative positions of the ^{1}MLCT excited state (accessible under visible irradiation) and of the dissociative triplet state will play an important role in the photodissociation mechanism of the ethyl complex. The presence of an ultra fast (a few hundred femtoseconds) concurrent carbonyl dissociation is not verified, but the situation depicted in Fig. 2(c) is favorable to an extremely efficient radical formation after ^{1}MLCT→^{3}(LLCT/MLCT) ISC.

3.3. Photodissociation dynamics of $HMn(CO)_3(DAB)$

3.3.1. Absorption spectrum

The theoretical absorption spectrum of $HMn(CO)_3(DAB)$ has been obtained through propagation of the selected $\Psi_{^1_cA'}(q_a, t)$ wavepacket on the $V_{^1_aA'}(q_a)$, $V_{^1_bA'}(q_a)$, $V_{^1_cA'}(q_a)$, $V_{^1_dA'}(q_a)$ and $V_{^1_eA'}(q_a)$ potentials corresponding to the excited states labelled in Table 1, under C_s symmetry constraint. The two lowest ^{3}MLCT states, a^3A' and b^3A' have been excluded from the simulation on the basis of preliminary propagations performed on the whole set of potentials. This simulation indicates a very low efficiency of the ISC process to these states. The evolution of the initial wavepacket has been followed by solving the fully coupled 5×5 diabatic Schrödinger equation (Eq. (9)), including diabatic potential coupling terms (Eq. (8)) coming either from singlet–triplet spin–orbit interaction or from kinetic coupling, with the following initial conditions:

$$\begin{aligned}
\Psi_{^1_bA'}(q_a, t=0) &= \mu_{^1_aA'\rightarrow{}^1_bA'}\Phi_{^1_aA',0}(q_a)\\
\Psi_{^1_cA'}(q_a, t=0) &= \mu_{^1_aA'\rightarrow{}^1_cA'}\Phi_{^1_aA',0}(q_a)\\
\Psi_{^1_dA'}(q_a, t=0) &= \mu_{^1_aA'\rightarrow{}^1_dA'}\Phi_{^1_aA',0}(q_a)
\end{aligned} \tag{10}$$

where $\mu_{i\rightarrow j}$ are the calculated dipole transition moments between the states i and j and

$$\Psi_{^3_cA'}(q_a, t=0) = 0 \tag{11}$$

The computed electronic absorption spectrum of $HMn(CO)_3(DAB)$, shown in Fig. 3, has been obtained with vibrational relaxation effects (dashed lines) and without them (solid lines).

The fine structure (solid lines) shows an intense and sharp peak centered at 26 000 cm^{-1} corresponding to the $a^1A'\rightarrow c^1A'$ absorption and several less intense narrow peaks in the region between 35 000 and 45 000 cm^{-1}. Among them, the most intense corresponding to the $a^1A'\rightarrow d^1A'$ transition is assigned to the ^{1}LLCT state. This series reflects the complex structure of the potentials in this high energy domain

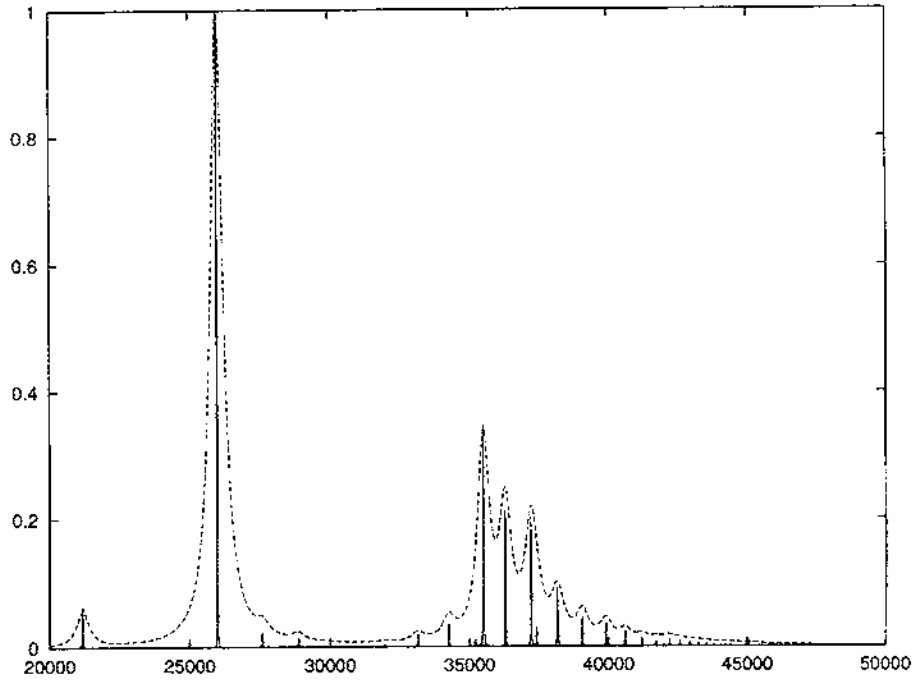

Fig. 3. Theoretical electronic absorption spectrum $S_{tot}(\omega)$ of $HMn(CO)_3(DAB)$, with vibrational relaxation effects included (dashed lines) and without the vibrational relaxation effects (solid lines).

(due to the mixing of the ^{1}LLCT state with other singlet states). A third peak of low intensity is detected at 21 000 cm^{-1} and corresponds to the weakly allowed $a^1A' \rightarrow b^1A'$ ^{1}MLCT transition. Inclusion of the vibrational relaxation effects in the simulation (by an exponential correction to the autocorrelation function) induces a broadening of the bands and obscures the fine structure in the theoretical absorption spectrum (Fig. 3: dashed line).

3.3.2. Visible photochemistry

In order to follow the photochemical behavior of $HMn(CO)_3(DAB)$ under irradiation in the visible, and to determine the role of the low-lying triplet states, we have performed one-dimensional wavepacket propagations along the q_a = Mn–H reaction coordinate. Five excited states have been selected on the basis of preliminary propagations performed on the whole set of electronically excited potentials: the low-lying b^1A' and c^1A' (^{1}MLCT) states (in the visible absorption domain) and the triplet a^3A', b^3A' (^{3}MLCT) and c^3A' (^{3}LLCT) excited states. Note that the c^3A' state leads to the H + $Mn(CO)_3(DAB)$ primary products [27–30]. The time evolution of the $\Psi_{^1_bA'}(q_a, t)$, $\Psi_{^1_cA'}(q_a, t)$, $\Psi_{^3_aA'}(q_a, t)$, $\Psi_{^3_bA'}(q_a, t)$ and $\Psi_{^3_cA'}(q_a, t)$ wavepackets has been followed by propagation on the corresponding potentials by solving sets of spin–orbit and non-adiabatically coupled time-dependent Schrödinger equations

(Eq. (9)) (see Section 3.3.1) with the following initial conditions:

$$\Psi_{^1_cA'}(q_a, t=0) = \mu_{^1_aA'\rightarrow{}^1_cA'}\Phi_{^1_aA',0}(q_a) \tag{12}$$

and

$$\Psi_{^1_bA'}(q_a, t=0) = \Psi_{^1_dA'}(q_a, t=0) = \Psi_{^3_aA'}(q_a, t=0) = \Psi_{^3_bA'}(q_a, t=0)$$
$$= \Psi_{^3_cA'}(q_a, t=0) = 0 \tag{13}$$

The corresponding snapshots of densities are shown in Fig. 4 and the probability of observing the primary reaction $HMn(CO)_3(DAB) \rightarrow H + Mn(CO)_3(DAB)$ is repre-

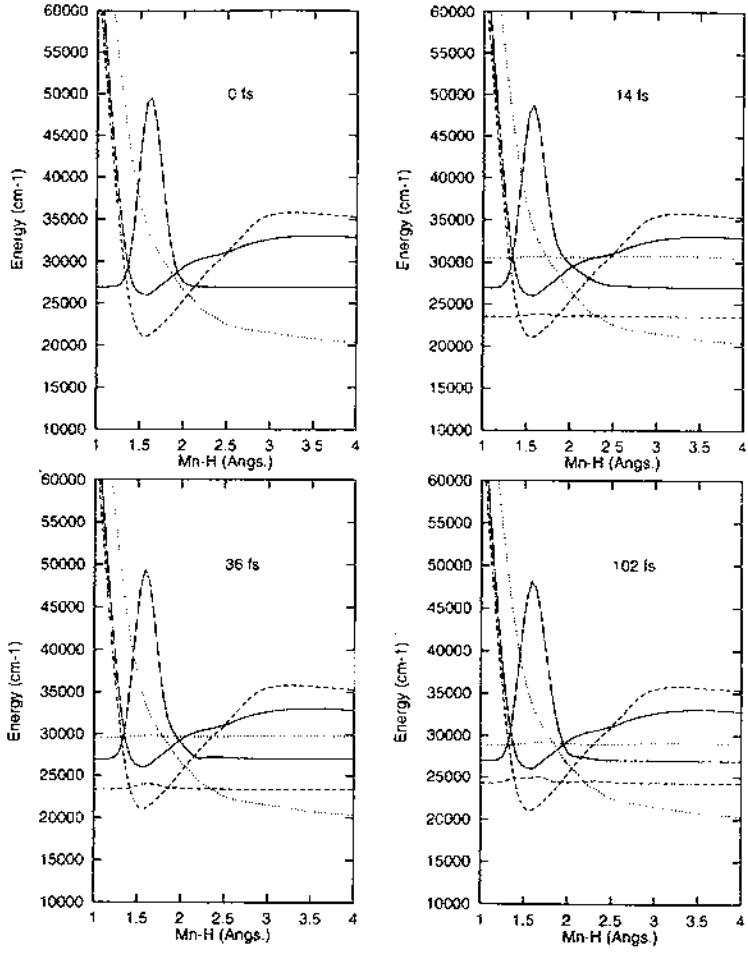

Fig. 4. Time evolution of the $\Psi_{^1_bA'}(q_a, t)$ (· · · ·), $\Psi_{^1_cA'}(q_a, t)$ (– · – · –) and $\Psi_{^3_cA'}(q_a, t)$ (·····) wavepackets on the spin–orbit and non-adiabatically coupled $V_{^1_bA'}(q_a)$ (– – –), $V_{^1_cA'}(q_a)$ (———) and $V_{^3_cA'}(q_a)$ (·····) potentials as a function of q_a = [Mn–H].

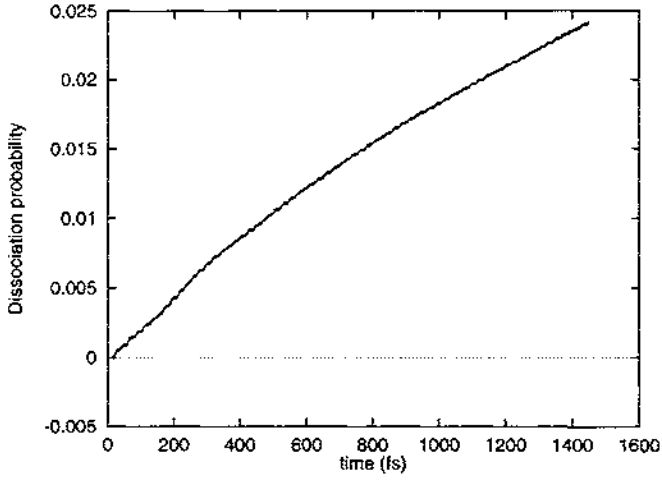

Fig. 5. Probability for observing the reaction $HMn(CO)_3(DAB) \rightarrow H + Mn(CO)_3(DAB)$ after irradiation in the visible.

sented in Fig. 5. For the sake of clarity, the two low-lying $V_{^3_aA'}(q_a)$ and $V_{^3_bA'}(q_a)$ are not represented in the snaphots.

Under irradiation in the visible region the system does not have enough energy to photodissociate in a short time scale. The major event is the trapping of the wavepacket in the low-lying ^{1}MLCT potential wells. In the picosecond time scale only 2% of the system dissociates to the primary products of the reaction in Eq. (2) (Fig. 5). This dissociative process occurs after ^{1}MLCT$\rightarrow^3$LLCT ISC, which is the rate-determining step. Immediately after the initial excitation, the ^{3}LLCT is weakly populated (less than 1%) and the small fraction of wavepacket coming from the singlet potential runs out toward the primary products $H + Mn(CO)_3(DAB)$ (^{1,3}A′) leading to diradicals.

3.3.3. *UV photochemistry*

In order to follow the photochemical behavior of $HMn(CO)_3(DAB)$ under irradiation in the UV energy domain, we have performed one-dimensional wavepacket propagations along the q_a = Mn–H reaction coordinate. Three excited states have been selected in this simulation: the d^1A' (^{1}LLCT) state, a second singlet state e^1A' (not reported in Table 1, but nearly degenerate with the ^{1}LLCT in the Franck–Condon region and corresponding mainly to a $3d_{yz} \rightarrow 3d_{xy}$ excitation) and the c^3A' (^{3}LLCT) state. The time evolution of the $\Psi_{^1_dA'}(q_a, t)$, $\Psi_{^1_eA'}(q_a, t)$ and $\Psi_{^3_cA'}(q_a, t)$ wavepackets has been followed by propagation on the corresponding potentials by solving sets of spin–orbit and non-adiabatically coupled time-dependent Schrödinger equations (Eq. (9)) (see Section 3.3.1) with the following initial conditions:

$$\Psi_{^1_dA'}(q_a, t=0) = \mu_{^1_aA' \rightarrow ^1_dA'} \Phi_{^1_aA',0}(q_a) \tag{14}$$

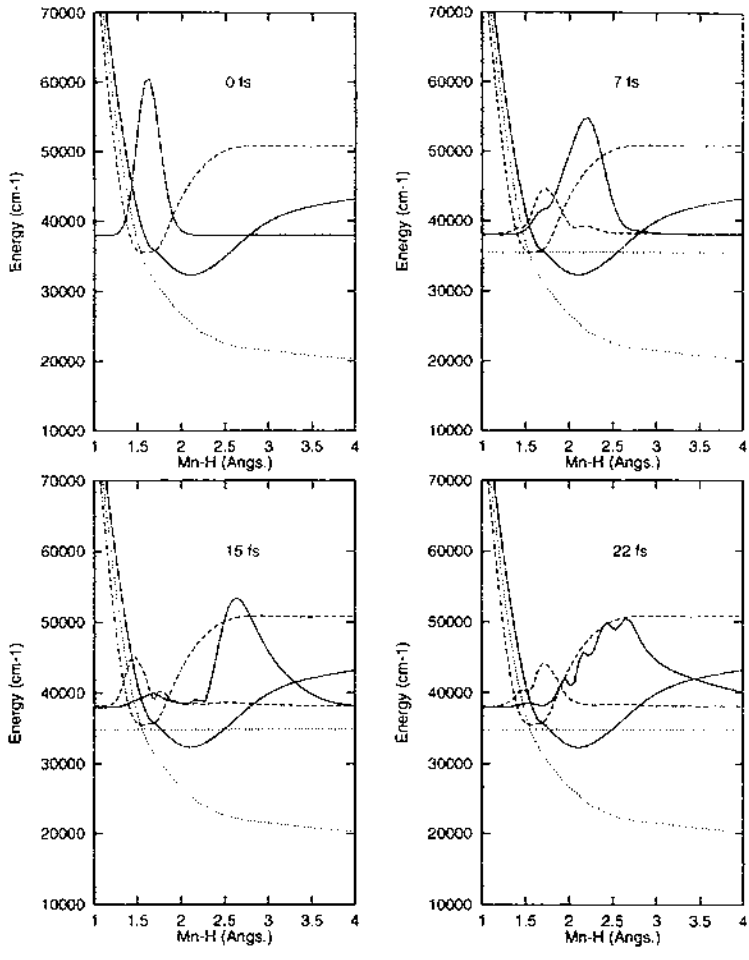

Fig. 6. Time evolution of the $\Psi_{^1_cA'}(q_a, t)$ (— ·—), $\Psi_{^2_cA'}(q_a, t)$ (– ––) and $\Psi_{^3_cA'}(q_a, t)$ (···) wavepackets on the spin–orbit and non-adiabatically coupled $V_{^1_dA'}(q_a)$ (— ·), $V_{^1_eA'}(q_a)$ (––) and $V_{^2_eA'}(q_a)$ (·····) potentials as a function of q_a=[Mn–H].

and

$$\Psi_{^1_cA'}(q_a, t=0) = \Psi_{^3_cA'}(q_a, t=0) = 0 \tag{15}$$

The corresponding snapshots of densities are shown in Fig. 6.

Under irradiation in the UV region, the system evolves between the two potential wells of the d^1A' and e^1A' excited states on both sides of the energy barrier around 1.75 Å, which is generated by avoided crossing between these states. In the first 10 fs around 20% of the wavepacket overcomes the barrier and evolves in the $V_{^1_cA'}(q_a)$ potential. The main part of the system remains on the initially populated ^{1}LLCT state, where it starts to dissociate towards H + Mn(CO)$_3$(DAB) (d^1A') primary

products. The population of the dissociative ^{3}LLCT state through ISC is negligible, since the crossing point between the singlet and triplet states is located at a rather short Mn–H distance (1.5 Å) where the amplitude of the initial wavepacket is too small to induce efficient transfer to the triplet state (the singlet–triplet spin–orbit coupling has a value of 10 cm^{-1} at the crossing point). However, in the limit of this one-dimensional simulation, the evolution of the wavepacket after 20 fs indicates that more favorable situations to ISC could occur in a longer time scale.

4. Conclusion

The photochemistry of a series of MLCT $RM(CO)_3(DAB)$ (M=Mn, R=H, methyl, ethyl; M=Re, R=H) complexes has been studied through quantum chemical calculations completed by simulation of the excited states dynamics in $HMn(CO)_3(DAB)$.

The influence of the ligand R on the sequence of excited states from the hydride to the ethyl complex is: (i) a significant lowering of the excited states, which is more pronounced for the LLCT states than for the MLCT states; (ii) an increase in the mixing between the low-lying ^{1}MLCT states, on the one hand, and between the ^{3}MLCT/^{3}LLCT states on the other hand. The state correlation diagrams enabled us to propose a qualitative mechanism of deactivation of $RMn(CO)_3(DAB)$ (R= H, methyl, ethyl) under irradiation in the visible; after efficient allowed transition to the higher ^{1}MLCT state, the system may either get trapped into the MLCT potential wells (R=H, methyl) or photodissociate towards the primary products $R+Mn(CO)_3(DAB)$ (R=ethyl). This mechanism accounts for the experimental findings recently reported for this class of molecules, namely no breaking of the Mn–methyl bond but an efficient Mn–benzyl bond homolysis in the $RMn(CO)_3(\alpha$-diimine) [1–9]. A comparative study of the lowest excited states in $HMn(CO)_3(DAB)$ and $HRe(CO)_3(DAB)$ has been undertaken. The low-lying excited states of $HMn(CO)_3(DAB)$ are nearly pure and range between 15 000 and 37 950 cm^{-1}, in contrast to its rhenium homologue in which the lowest part of the spectrum is characterized by mixed LLCT/MLCT states between 12 600 and 31 34 0 cm^{-1}.

The main features of the absorption spectra of $HMn(CO)_3(DAB)$ have been reproduced, in the limit of the one-dimensional propagation of selected wavepackets on spin–orbit and non-adiabatically coupled ^{1,3}LLCT and ^{1,3}MLCT potentials. The intense and sharp peak in the visible domain of energy has been assigned to the second $a^1A' \rightarrow c^1A'$ (MLCT) transition, whereas several less intense narrow bands in the UV region have been attributed to the weakly bound ^{1}LLCT state. The simulation of the visible photochemistry, by propagation of selected wavepacket initially placed on the low-lying singlet MLCT states, does not show any efficient homolysis. In contrast, the major event is the trapping of the system into the ^{1}MLCT potential wells. Surprisingly, propagation along the Mn–H bond elongation after excitation in the appropriate domain of energy (30 000–38 000 cm^{-1}) shows that the UV photochemistry is not efficient. The wavepacket evolves between the

two potential wells of the singlet states on both sides of the energy barrier located around 1.75 Å. The main part of the system gets trapped into the ^{1}LLCT potential well from which a negligible part begins to dissociate slowly to the $H+Mn(CO)_3(DAB)$ primary products. The singlet–triplet ISC processes seem to play a minor role in the femtosecond dynamics of $HMn(CO)_3(DAB)$ excited states. However, efficient singlet to triplet transitions should not be excluded at a longer time scale.

Further work is oriented towards the two-dimensional simulation of the photodissociation dynamics, including the Mn–CO elongation, in order to study the concurrent primary reaction leading to the CO dissociation observed in a few $MeMn(CO)_3$(α-diimine) complexes [1–9]. A complete study of the spin–orbit interactions in the excited states of $HRe(CO)_3(DAB)$ is necessary to investigate the influence of the metal center on the photochemical behavior in this class of molecules. We hope to have shown that a step forward in the understanding of the photodissociation dynamics in the MLCT complexes is the development of sophisticated experimental techniques able to provide information at the early stage of the photodissociation.

Acknowledgements

The authors are grateful to Professor D.J. Stufkens for stimulating discussions and to Dr. M.C. Heitz who initiated the dynamics in Strasbourg and to Dr. P. Saalfrank and Dr. C. Ribbing for the development of new formalisms related to the coupling problems. We thank J.L. Heully and M. Dolg for their collaboration in the handling of the effective core potentials. Generous financial support by the PROCOPE French/German projects 93207 and the Euronetwork "Quantum Chemistry on Transition Metal Complexes" No. ERBCHRXCT 930156 is gratefully acknowledged. M.R.H. thanks the Chateaubriand Canadian/French fellowship. The quantum ab initio calculations have been carried out on the Cray-2 computer of the C98 computer of the IDRIS (Orsay, France) through a grant of computer time from the Conseil Scientifique. The quantum dynamics have been performed on the workstations at the Institute für Physikalische und Theoretische Chemie, Freie Universität (Berlin) and at the Laboratoire de Chimie Quantique, CNRS (Strasbourg).

References

[1] D.J. Stufkens, Comments Inorg. Chem. 13 (1992) 359.
[2] D.J. Stufkens, Coord. Chem. Rev. 104 (1990) 39.
[3] B.D. Rossenaar, T. van der Graaf, R. van Eldick, C.H. Langford, D.J. Stufkens, A. Vlček Jr., Inorg. Chem. 33 (1994) 2865.
[4] B.D. Rossenaar, C.J. Kleverlaan, D.J. Stufkens, A. Oskam, J. Chem. Soc. Chem. Commun. (1994) 63.
[5] J.W.M. van Outerstep, D.J. Stufkens, A. Vlček Jr., Inorg. Chem. 34 (1995) 5183.

[6] B.D. Rossenaar, M.W. George, F.P.A. Johnson, D.J. Stufkens, J.J. Turner, A. Vlček Jr., J. Am. Chem. Soc. 117 (1995) 11582.
[7] B.D. Rossenaar, C.J. Kleverlaan, M.C.E. van de Ven, D.J. Stufkens, A. Vlcek Jr., Chem. Eur. J. 2 (1996) 228.
[8] B.D. Rossenaar, D.J. Stufkens, A. Oskam, J. Fraanje, K. Goubitz, Inorg. Chim. Acta 247 (1996) 215.
[9] B.D. Rossenaar, E. Lindsay, D.J. Stufkens, A. Vlcek Jr., Inorg. Chim. Acta 250 (1996) 5.
[10] H. Hermann, F.W. Grevels, A. Henne, K. Schaffner, J. Phys. Chem. 86 (1982) 5156.
[11] J.N. Moore, P.A. Hansen, R.M. Hochstrasser, Chem. Phys. Lett. 138 (1987) 110.
[12] J.N. Moore, P.A. Hansen, R.M. Hochstrasser, J. Am. Chem. Soc. 111 (1989) 4563.
[13] P.A. Anfirud, C.H. Han, T. Lian, R.M. Hochstrasser, J. Phys. Chem. 95 (1991) 574.
[14] L. Wang, X. Zhu, K.G. Spears, J. Am. Chem. Soc. 110 (1988) 8695.
[15] L. Wang, X. Zhu, K.G. Spears, J. Phys. Chem. 93 (1989) 2.
[16] J. Zhang, D.G. Imre, Chem. Phys. Lett. 149 (1988) 233.
[17] J. Zhang, D.G. Imre, J.H. Frederick, J. Phys. Chem. 93 (1989) 1840.
[18] D. Chasman, D.G. Imre, D.J. Tannor, J. Chem. Phys. 89 (1988) 6667.
[19] D.G. Imre, J. Zhang, J. Chem. Phys. 139 (1989) 89.
[20] J. Zhang, E.J. Heller, D. Huber, D.G. Imre, D.J. Tannor, J. Chem. Phys. 89 (1988) 3602.
[21] C. Daniel, M.C. Heitz, L. Lehr, T. Schröder, B. Warmuth, Int. J. Quant. Chem. 52 (1994) 7.
[22] C. Daniel, E. Kolba, L. Lehr, T. Schröder, J. Manz, J. Phys. Chem. 98 (1994) 9823.
[23] C. Daniel, M.C. Heitz, J. Manz, C. Ribbing, J. Chem. Phys. 102 (2) (1995) 905.
[24] M.C. Heitz, C. Ribbing, C. Daniel, J. Chem. Phys. 106 (4) (1997) 1421.
[25] M.C. Heitz, K. Finger, C. Daniel, Coord. Chem. Rev. 159 (1997) 171.
[26] M.C. Heitz, C. Daniel, J. Am. Chem. Soc. 119 (1997) 8269.
[27] K. Finger, C. Daniel, J. Chem. Soc. Chem. Commun., (1995) 1427.
[28] K. Finger, C. Daniel, J. Am. Chem. Soc. 117 (1995) 12322.
[29] K. Finger, C. Daniel, P. Saalfrank, B. Schmidt, J. Phys. Chem. 100 (1996) 3368.
[30] K. Finger, Ph.D. Thesis, Berlin, 1996.
[31] G.S. Schmidt, H. Paulus, R. van Eldik, H. Elias, Inorg. Chem. 27 (1988) 3211.
[32] E.A. McNeill, F.R. Scholer, J. Am. Chem. Soc. 99 (1977) 6243.
[33] D. Guillaumont, M.P. Wilms, C. Daniel, D.J. Stufkens, submitted to Inorg. Chem.
[34] D. Guillaumont, C. Daniel, Chem. Phys. Lett. 257 (1996) 1.
[35] G. Guillaumont, C. Daniel, submitted to Chem. Phys. Lett.
[36] P.E.M. Siegbahn, J. Almlöf, A. Heiberg, B.O. Roos, J. Chem. Phys. 74 (1981) 2384.
[37] P.E.M. Siegbahn, Int. J. Quant. Chem., 23 (1983) 1869
[38] D. Andrae, U. Haeussermann, M. Dolg, H. Stoll, H. Preuss, Theor. Chim. Acta 77 (1990) 123.
[39] A. Bergner, M. Dolg, W. Kuechle, H. Stoll, H. Preuss, Mol. Phys. 80 (1993) 1431.
[40] A. Veillard, A. Dedieu, New J. Chem. 7 (1983) 683.
[41] A. Veillard, A. Dedieu, Theo. Chim. Acta 63 (1983) 339.
[42] C. Daniel, A. Veillard, New J. Chem. 10 (1986) 83.
[43] N.J. Turro, Modern Molecular Photochemistry, Benjamin/Cummings, Menlo Mark, CA, 1978.
[44] D. Guillaumont, C. Daniel, P. Saalfrank, in preparation.
[45] R. Meyer, J. Chem. Phys. 52 (1969) 2053.
[46] C.C. Morston, C.G. Balint-Kurti, J. Chem. Phys. 91 (1989) 3571.
[47] D. Kosloff, R. Kosloff, J. Comput. Phys. 52 (1983) 35.
[48] C. Ribbing, C. Daniel, J. Chem. Phys. 100 (1994) 6591.
[49] B.D. Rossenaar, Ph.D. Thesis, Universiteit van Amsterdam, Netherlands, 1995.